Bulk and in-gap states in SmB_6 revealed by high-field magnetotransport

M. Shahrokhvand,* S. Pezzini, M. R. van Delft, U. Zeitler, N. E. Hussey, and S. Wiedmann†
High Field Magnet Laboratory (HFML-EMFL), Radboud University, Toernooiveld 7, 6525 ED Nijmegen, The Netherlands and Radboud University, Institute of Molecules and Materials, Heyendaalseweg 135, 6525 AJ Nijmegen, The Netherlands
(Received 18 July 2017; revised manuscript received 17 October 2017; published 14 November 2017)

We report on temperature-dependent magnetotransport experiments of SmB_6 single crystals in high magnetic fields up to 33 T. Above the low-temperature plateau region in the zero-field resistivity, we find two distinct gapped regimes. The first is characterized by a temperature-independent gap Δ_2 that closes in the presence of a high magnetic field while the second regime, above ~8 K, features an energy gap Δ_1 that is temperature dependent. In the entire temperature range, we observe an overall negative magnetoresistance that does not depend on the orientation of the crystalline plane with respect to the applied magnetic field with a maximum value at $T \sim 6.2$ K. The regime of in-gap states is characterized by a low mobility, an anomalously high carrier concentration, and an enhanced nonlocal resistance that exceeds the expected classical value for a two-dimensional metallic conductor. Overall, our data can be interpreted in terms of a transition from bulk to in-gap dominated transport, but evidence of topological surface states is not observed.

DOI: 10.1103/PhysRevB.96.205125

I. INTRODUCTION

So far, topological insulators (TIs), i.e., band-inverted insulators with topologically protected conducting surface states, have been realized in weakly interacting electron systems [1–3]. However, new physical phenomena are expected to arise from the combination of topological character and strong many-body interactions. SmB_6, a well-known Kondo insulator (KI), is an intermediate valence compound with CsCl-type crystal structure. At high temperatures, the valence ($4f$) and conduction electrons ($5d$) of the samarium ions are decoupled and its resistivity has only a weak temperature dependence. With decreasing temperature, a small energy gap, known as the Kondo gap, due to hybridization of the $4f$ and $5d$ electrons, appears at the Fermi level. While this gap opening is responsible for an initial divergence of the resistivity, the experimental observation of a saturating resistivity at the lowest temperatures (<4 K) remained a mystery for more than 30 years. Recently, theoretical calculations [4–6] have suggested that such Kondo insulators can also be topological insulators, defining a new class of materials called topological Kondo insulators (TKIs), which differ from conventional TIs owing to the many-body origin of the bulk band gap. Motivated by theoretical calculations, successive experimental works [7–21] have been carried out to confirm whether the low-temperature plateau in the electrical resistivity of SmB_6 is due to the topological surface states (TSS). So far, the existence of in-gap states has been revealed by different techniques such as transport [7,10,11,14–17] and angle-resolved photoemission spectroscopy (ARPES) [12,13,19]. Although mostly these in-gap states have been attributed to the TSS [12,14–16,19], their exact nature remains controversial [20,21]. Unlike the situation in other TIs such as Bi_2Te_3 [22] or HgTe [23], the topological character of the surface states in SmB_6 has not yet been established experimentally, although this could be due to the limited resolution of the existing ARPES setups [20]. At the same time, evidence for in-gap states of a trivial nature, i.e., due to Rashba splitting, has also been reported in Ref. [21]. Nevertheless, the vast majority of active researchers in this field claim that the observation of the resistance plateau at low temperature is due to TSS and hence SmB_6 is presumed to be the first TKI [8,12,13,19].

In this work, we investigate the magnetoresistance (MR) and Hall resistance of SmB_6 single crystals at different temperatures in magnetic fields up to 33 T. We have characterized an ensemble of samples with different dimensions and inverse resistance ratio (IRR) up to 8300. The IRR is defined as the ratio between the residual resistance at 1.3 K and the resistance at room temperature, [IRR $= R(1.3\text{ K})/R(300\text{ K})$]. With increasing temperature, we find evidence for two distinct energy gaps, one of which, the field-dependent gap Δ_2, is found to be the origin of the observed negative MR. The regime of in-gap states is characterized by a low mobility, a high carrier concentration, and nonlocal resistance that exceed the expected classical value for a two-dimensional metallic conductor. Unless otherwise specified, all the data in this paper were taken with a magnetic field applied perpendicular to the crystallographic plane while the field was always applied perpendicular to the current path.

II. EXPERIMENTAL TECHNIQUES

High-quality SmB_6 single crystals were grown by the Al-flux method using samarium pieces (99.9%), boron powder (99.99%), and aluminium pieces with a ratio of 0.5 g of Sm:B (1:6) and 50 g of Al (99.99%). The growth was performed in a vertical gradient furnace under a continuous flow of argon at temperatures up to 1500 °C with a cooling rate of 5 Kh^{-1}. To remove the aluminium flux, the samples were cleaned by a potassium hydroxide solution [12]. Electrical contacts were made onto several macroscopic samples by conducting Ag paste using 25-μm gold wires in a Hall-bar geometry [see Fig. 1(e)]. In addition, one sample (S6) was shaped by focused ion beam (FIB) and the electrical contacts were made by FIB-induced platinum deposition [Fig. 1(f)]. Standard four-probe resistance experiments were performed as

*maryam.shahrokhvand@ru.nl
†steffen.wiedmann@ru.nl

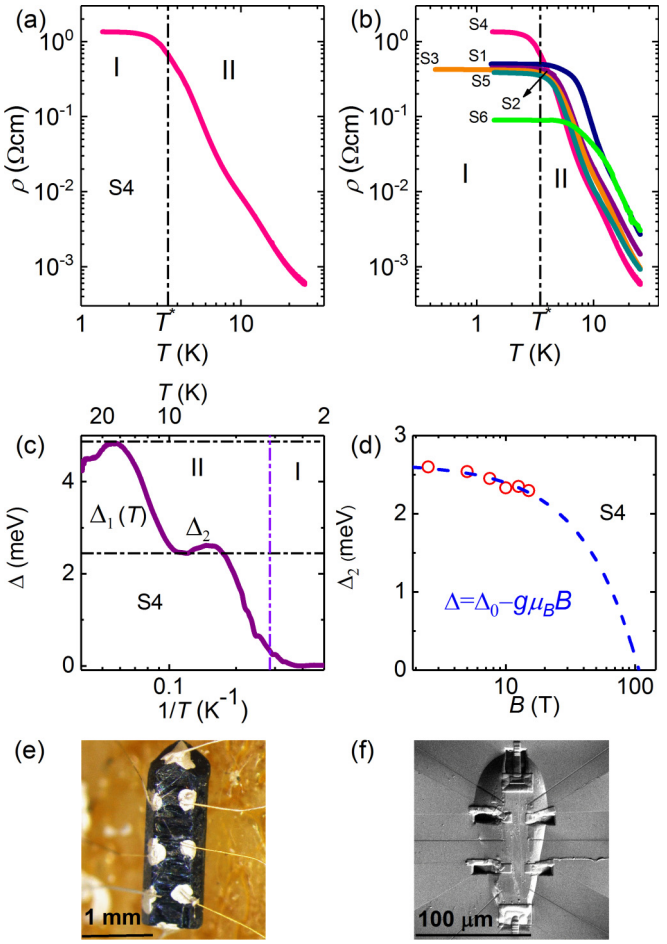

FIG. 1. (a) Temperature dependence of the resistivity for sample S4 from 1.3 to 25 K. (b) Temperature dependence of the resistivity for different samples. (c) Temperature dependence of the two gaps derived from the temperature dependence of the resistance in a semilog plot. (d) Field dependence of the Kondo gap. The blue dashed line is the linear extrapolation on a semilogarithmic scale which gives the critical field for Δ_2. (e) Image of sample S4 with the electrical contacts. (f) Scanning electron microscopy image of the FIB-processed sample S6.

a function of magnetic field ($B = 0$ to 33 T) and temperature ($T = 0.4$ to 25 K) in both Bitter and superconducting magnets. A summary of all samples used in this study is given in Table I.

TABLE I. Dimension [thickness (T), width (W), and length (L)] and inverse resistance ratio (IRR) for all samples.

Sample	Dimension (T, W, L) mm	IRR
S1	(0.7, 0.73, 1.1)	1600
S2	(0.7, 0.73, 1.37)	1250
S3	(0.7, 0.73, 1.84)	1550
S4	(0.7, 0.73, 1.48)	8300
S5	(0.64, 0.87, 1.08)	1000
S6	(0.009, 0.021, 0.048)	178

III. EXPERIMENTAL RESULTS

At zero magnetic field, we observe a strong increase in the resistivity ρ of the crystals studied by several orders of magnitude with decreasing temperature, as illustrated in Figs. 1(a) and 1(b). Two different regimes can be identified from the temperature dependence of the resistivity. In regime II, the resistivity increases exponentially with decreasing temperature from ∼25 to 3.5 K, as a small gap appears at the Fermi level [4]. However, below $T^* \sim 3.5$ K, the resistivity saturates (regime I). As shown in Fig. 1(b), this behavior was reproduced in all six samples studied with different length, width, and thickness. In the microfabricated sample (S6), the magnitude of the resistivity plateau was found to be significantly smaller than the macroscopic samples which likely originates from a parallel conduction channel formed in the FIB processing [24]. In general, the variation in IRR values reflects different levels of disorder or off-stoichiometry [25]. In sample S3, the low-temperature plateau in the resistivity exists down to 0.4 K.

We now turn our attention to the Kondo gap. Unlike a conventional band gap, the Kondo gap is strongly temperature dependent and opens only below the Kondo temperature T_K [26]. From the temperature dependence of the resistance $R \propto \exp(\Delta/k_B T)$, we extract the Kondo gap as $\Delta = k_B d \ln[(R)/d(1/T)]$. Thus, by plotting the first derivative of the logarithmic resistance versus $1/T$, we can follow the evolution of the Kondo gap with temperature. The opening of the gap can be clearly seen as the material is cooled down below ∼25 K. In agreement with previous results [7,27], two gaps can be identified [see Fig. 1(c)]. Although the dependence on the magnetic field has been addressed [7], the nature of $\Delta(T)$ has yet to be explored. With decreasing temperature, the Kondo gap increases as expected until ∼17 K, whereupon it decreases and eventually becomes constant at a value approximately half of the original Kondo gap between 8 and 5 K [see Fig. 1(c)]. This two-gap behavior cannot be explained through the simple hybridization between the conduction and valence electrons which should yield only one gap. Therefore, it is likely that the level mixing in SmB_6 is more complex than what is expected in the standard hybridization model. The observed "two-gap behavior" can be addressed by considering both strong spin-orbit coupling and crystal-field splitting of the f states of Sm into several multiplets [28]. The multiplet f states hybridize with the Sm d band at different energies, resulting in the opening of two gaps at different temperatures, in agreement with our observations, one at higher temperature, $\Delta_1(T)$ from ∼8 to 25 K, that is strongly temperature dependent and one, Δ_2, that is temperature independent in the range from ∼5 to 8 K. Below 3.5 K, we enter the plateau region of saturating resistance where in-gap states determine the observed transport properties. This behavior was reproduced in different samples studied and the data are shown in Fig. 5(a) of the Appendix.

In order to provide more information about this two-gap behavior, we have measured the resistance as a function of temperature in a constant perpendicular magnetic field and extracted the resultant values for $\Delta_1(T)$ and Δ_2. The field reduction of the Kondo gap can be explained by the Zeeman effect with [29]

$$\Delta(B) = \Delta_0 - g\mu_B B. \quad (1)$$

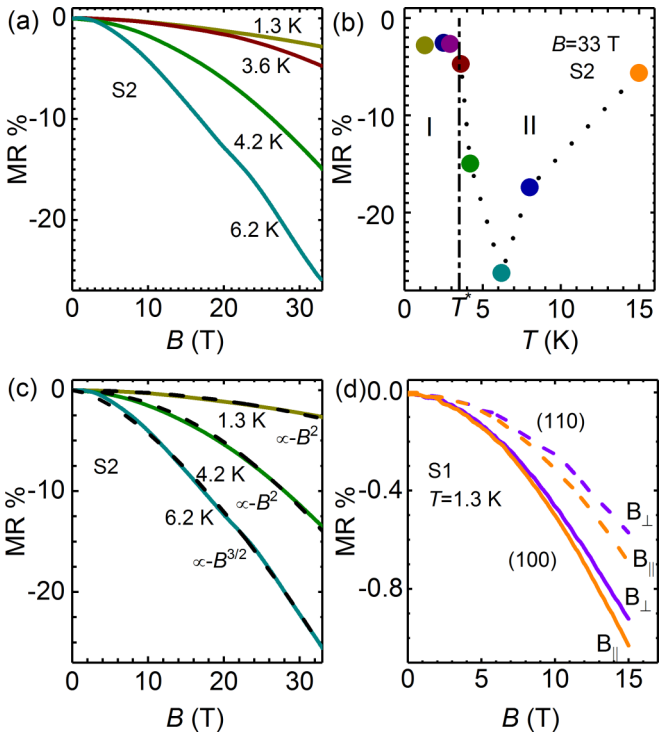

FIG. 2. (a) Magnetoresistance for sample S2 at some fixed temperatures in perpendicular magnetic fields up to 33 T. (b) Temperature dependence of the MR at $B = 33$ T. (c) The MR for sample S3 along with their best fits. The MR at $T = 1.3$ and 4.2 K are proportional to $-B^2$ while one at 6.2 K is proportional to $-B^{3/2}$. (d) The angle dependence of the MR for both (110) and (100) surfaces of the sample S1 at $T = 1.3$ K.

where μ_B is the Bohr magneton, g is the Lande's g factor, Δ_0 is the gap at zero magnetic field, and B is the magnetic field. From Eq. (1), the evolution of the two gaps in a magnetic field can be traced and the critical field for the gap closure can be extracted. The blue dashed line in Fig. 1(d) is the corresponding fit to Eq. (1) for Δ_2, yielding a complete gap closure at a critical field $B_c \sim 107$ T, much beyond the ones at our disposal and consistent with previous studies [7,30]. This gap closure has been measured in YbB_{12} [31] and $Ce_3Bi_4Pt_3$ [32] and can be considered as a common feature of Kondo insulators. On the other hand, our data on $\Delta_1(T)$ do not show any significant field dependence which might be due to its higher mixing strength [31] and lack of resolution due to the relatively low magnetic field applied in this study [see Appendix, Fig. 5(b)].

We have also measured the magnetoresistance $\mathrm{MR} = [R_{xx}(B) - R_0]/R_0$ at fixed temperature and in high magnetic fields up to 33 T. Figure 2(a) shows the MR for sample S2 at 1.3, 3.6, 4.2, and 6.2 K. The first notable feature is a pronounced negative MR observed for all temperatures. For temperatures below 15 K [see Fig. 2(b)], the negative MR becomes more pronounced. Moreover, its magnitude continuously increases in the Δ_2 region with the highest value at ~6.2 K. With further decreasing temperature below 6.2 K, the amplitude of the negative MR rapidly decreases and, finally, in the regime dominated by the in-gap states below T^*, the MR is strongly suppressed. These results show that the negative MR has its maximum in the intermediate temperature range between ~5 to 8.5 K due to the field dependence of Δ_2. Another difference between the high- and low-temperature MR is its dependence on magnetic field. Figure 2(c) shows best fits to the the MR for sample S2 for selected temperatures in regimes I and II. As indicated by the dashed lines, a quadratic function fits the low-temperature part at 1.3 and 4.2 K quite well, but for $T >$ 4.2 K the MR more closely follows a $-B^{3/2}$ dependence.

As mentioned above, the observation of a negative MR has been reported in number of studies [7,9,30,33]. A possible scenario for the origin of this negative MR is a bulk gap closure due to Zeeman splitting [8]. Within this picture, Zeeman splitting decreases spin scattering of the Kondo lattice and eventually reduces the bulk Kondo gap resulting in the observed negative MR. This is consistent with our results in Fig. 1(d), which shows a linear decrease of Δ_2 with increasing magnetic field.

In order to distinguish between Zeeman splitting and orbital effects, we have measured the MR in both the parallel and perpendicular configurations. Here, parallel (perpendicular) configuration refers to a situation where the magnetic field is parallel (perpendicular) to the crystallographic plane on which the voltage contacts are placed. The results for sample S1, where we had electrical contacts on both the (110) and (100) surfaces, are shown in Fig. 2(d). The MR does not show a clear angle dependence either for (110) or for the (100) surface in contrast to the visible large-angle dependence in a sample with Corbino geometry [9].

In order to get further insight into the carrier concentration, we measured the Hall coefficient R_H from 1.3 to 17 K at $B = 15$ T. The Hall coefficient in regimes I and II is shown in Fig. 3(a). In regime I, below T^*, the Hall coefficient decreases with decreasing temperature. Above T^*, in regime II, R_H decreases with increasing temperature and has its maximum at 3.5 K in agreement with Refs. [10,34–36]. The spread of values of the crossover temperature T^* reported in the literature might be due to variation in sample quality.

The carrier concentration is found to exhibit two distinct behaviors depending on whether the bulk or the in-gap states dominate [see Fig. 3(b)]. From 17 to ~3.5 K, the carrier concentration decreases with decreasing temperature until all bulk carriers are frozen around $T^* = 3.5$ K. This is consistent with the Kondo scenario and the opening of the bulk band gap at the Fermi level. With further reduction in temperature below T^*, where the contribution from the in-gap states is expected to dominate, the carrier concentration recovers and eventually becomes temperature independent below ~2 K. The extracted carrier concentration in the regime dominated by in-gap states is $\sim 10^{17}$ cm^{-2} which is anomalously large for a 2D state and, therefore, in Fig. 3(b) we report the carrier concentration in units of cm^{-3}.

The Hall mobility μ is estimated from $\sigma = ne\mu$, and is plotted as the red curve in Fig. 3(b). The mobility is small at high temperature and increases slightly with decreasing temperature between 16 and ~8.5 K. From ~8.5 to 3.5 K, however, μ shows an unexpected decrease. This decrease is much more pronounced below 3.5 K until eventually it saturates below ~2 K. Interestingly, the peak in the mobility ~8.5 K corresponds to the kink in the carrier concentration in the region where the field-dependent gap Δ_2 resides. To the best of our knowledge, there are only two previous reports of

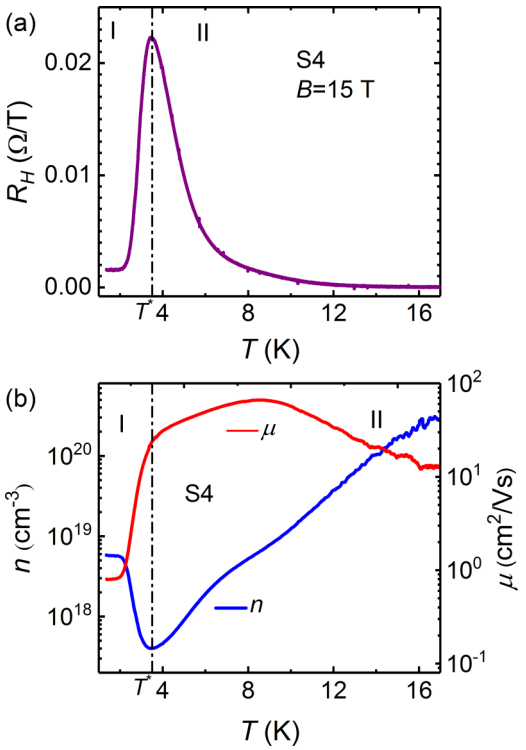

FIG. 3. (a) The temperature dependence of the Hall coefficient from $T = 1.3$ to 17 K. (b) The blue and red curves are the temperature dependence of the carrier concentration and the mobility from $T = 1.3$ to 17 K, respectively.

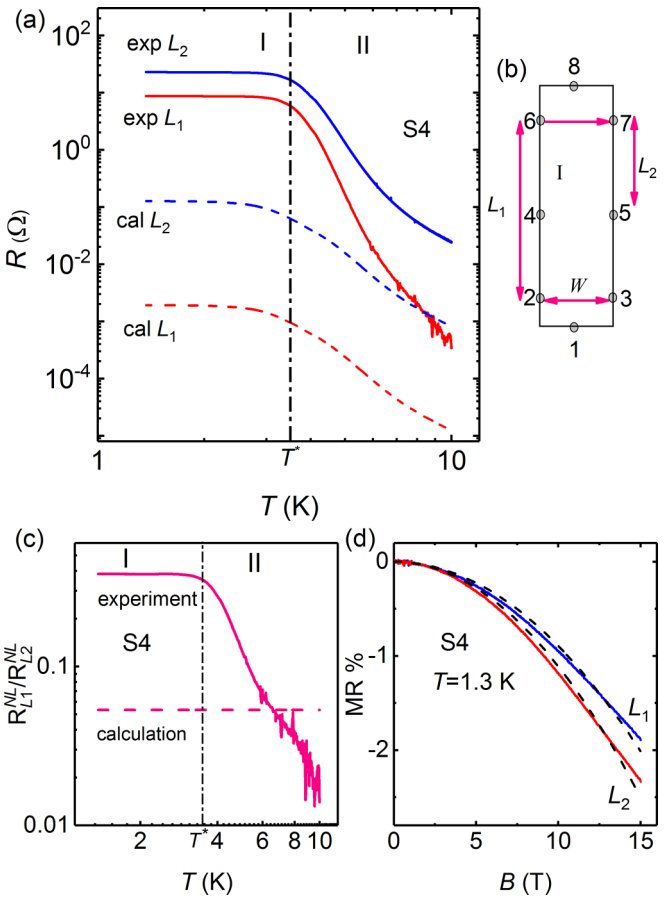

FIG. 4. (a) Temperature dependence of the nonlocal resistance from $T = 1.3$ to 10 K. The solid red and blue curves are the experimental nonlocal resistance for L_1 and L_2, respectively, while the dashed curves are the calculated ones according to Eq. (2). (b) Schematics of the sample's configuration for this measurement with $L_1 = 1500$ μm, $L_2 = 630$ μm, $W = 530$ μm. (c) Comparison between the experimental and the calculated R^{NL}_{L1}/R^{NL}_{L2}. (d) The nonlocal MR for two different distances from the current source, L_1 and L_2, along with the quadratic fit at $T = 1.3$ K.

the mobility in SmB_6 [9,11], both measured on samples in a Corbino geometry. Both reports are roughly in agreement with the value determined for our sample at ~8.5 K. The low value of mobility in regime I also explains the absence of quantum oscillations from the in-gap states in the MR up to 33 T.

The saturation of the resistivity in SmB_6 at low temperature has been attributed to the presence of surface states [4,6,12–16,37–39] and the observation of a nonlocal resistance signal to the TSS [10,17,18]. In a three-dimensional (3D) TI, if the Fermi energy is in the bulk band gap, the only conducting path is expected to be the two-dimensional (2D) metallic surface states, which results in easily computable nonlocal signals. For diffusive transport in a homogeneous 2D conductor, a nonlocal resistance is expected across voltage contacts located far away from the current path that decays exponentially with the distance from the current contacts at a rate set by the sample geometry [40]:

$$R_{nl} = \rho_{xx}\exp\left(-\pi\frac{L}{W}\right). \tag{2}$$

In this equation, ρ_{xx} is the resistivity of the material [as illustrated in Fig. 1(a)], W is the distance between the two voltage contacts, and L is the distance between the voltage and current contacts [see Fig. 4(b)]. To check this hypothesis, we performed nonlocal measurements for sample S4 from $T = 1.3$ to 10 K. Current was passed between contacts 6 and 7 and the voltage measured for two different distances from the current source: L_1 for contacts (2, 3) and L_2 for contacts (4, 5). The solid red and blue curves in Fig. 4(a) are the experimental nonlocal resistance curves for L_1 and L_2, respectively, while the dashed curves are the calculated curves according to Eq. (2).

The most striking observations from Fig. 4(a) are the strong enhancement of the nonlocal resistance below T^*, where the in-gap states reside, and the strong suppression above T^*, especially for the pair of contacts that are situated furthest from the current path L_1. To clarify this, we plot in Fig. 4(c) the ratio of the R^{NL}_{L1}/R^{NL}_{L2} from both experiment and model. Importantly, this ratio is expected to be a purely geometrical property, while being independent of the resistivity of the sample and its evolution with temperature. It is clear from Fig. 4(c) that the T dependence of the experimental and calculated ratios are completely different. Below T^*, R^{NL}_{L1}/R^{NL}_{L2} saturates with a value which is almost one order of magnitude larger than what is expected for a two-dimensional homogeneous metallic conductor. Moreover, the unexpected temperature dependence of the ratio signal R^{NL}_{L1}/R^{NL}_{L2} signifies that a dramatic change in the transport mechanism takes place in the transition between

regimes I and II. Consequently, we attribute the enhancement of the nonlocal resistance to the in-gap states as the system is tuned from bulk-dominated to in-gap dominated transport with decreasing temperature. The observed nonlocal resistance in SmB_6 is larger than what we expect for a 2D homogeneous metallic surface. This observation, together with the estimated carrier density and mobility, does not support the TSS character attributed in other works.

To probe the effect of the magnetic field on the nonlocal resistance, we have measured the nonlocal MR in magnetic fields up to 15 T. The symmetrized nonlocal MR at $T = 1.3$ K is shown in Fig. 4(d) for both L_1 and L_2 along with the quadratic fit for comparison (dashed lines). The nonlocal MR is small, negative, symmetric, and quadratic in field with a magnitude that is almost identical to the MR observed from local measurements and shown in Fig. 2(a).

IV. CONCLUSION

In conclusion, we have investigated the magnetotransport of SmB_6 single crystals in high magnetic fields up to 33 T. The temperature dependence of the resistivity can be divided into bulk- and in-gap dominated regimes. This behavior is reproducible and sample independent. Two distinct gaps with different temperature and field dependencies are revealed. The MR is negative and angle independent in both regimes and attributed to the field-dependent Kondo gap. Finally, we could not find any evidence of TSS in our magnetotransport measurements. The reason for the large disparity in the conclusions of different experimental studies is not known at this time, but clearly calls for further, more systematic investigation.

ACKNOWLEDGMENTS

We acknowledge N. Xu for fruitful discussions and for providing the SmB_6 crystals. This work was performed at the HFML-RU/FOM member of the European Magnetic Field 318 Laboratory (EMFL). It is part of the NWO Physics focus group 132: High Field Magnet Laboratory: a global player in science in high magnetic fields funded by the Netherlands Organization for Scientific Research (NWO).

APPENDIX

To confirm the reproducibility of the two-gap behavior, we show in Fig. 5(a) the T dependence of the extracted gaps for different samples. The gaps for four different samples show the same evolution with temperature, although their absolute values slightly differ. Moreover, to check the field dependence of these two gaps, we have measured the resistance as a function of temperature in constant perpendicular magnetic fields up to 15 T. As illustrated in Fig. 5(b), Δ_2 decreases with increasing magnetic field from which we extracted the data shown in Fig. 1(d) at 7 K. On the other hand, $\Delta_1(T)$ does not show any clear field dependence.

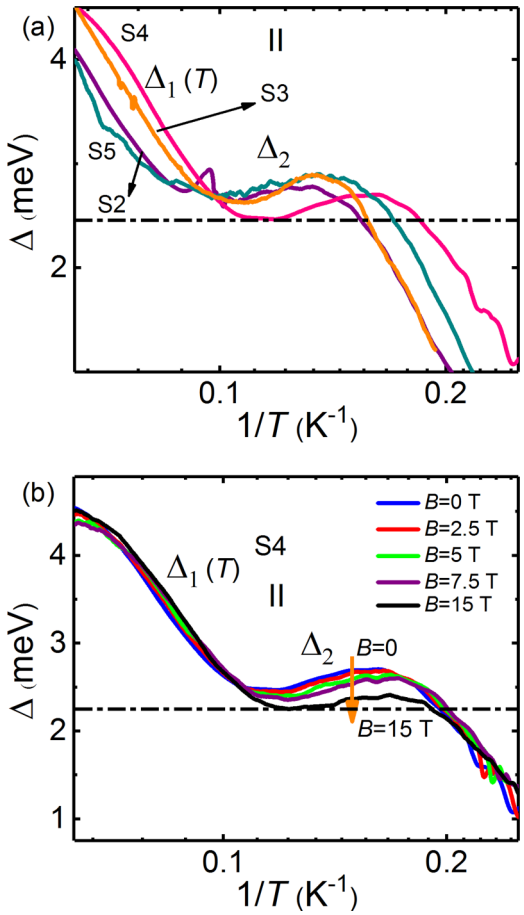

FIG. 5. (a) Temperature dependence of the Kondo gap for different samples. (b) Temperature dependence of the Kondo gap for sample S4 at several constant perpendicular magnetic fields.

[1] X.-L. Qi and S.-C. Zhang, Rev. Mod. Phys. **83**, 1057 (2011).
[2] L. Fu and C. L. Kane, Phys. Rev. B **76**, 045302 (2007).
[3] M. Z. Hasan and C. L. Kane, Rev. Mod. Phys. **82**, 3045 (2010).
[4] M. Dzero, K. Sun, V. Galitski, and P. Coleman, Phys. Rev. Lett. **104**, 106408 (2010).
[5] M. Dzero, K. Sun, P. Coleman, and V. Galitski, Phys. Rev. B **85**, 045130 (2012).
[6] T. Takimoto, J. Phys. Soc. Jpn. **80**, 123710 (2011).
[7] F. Chen, C. Shang, Z. Jin, D. Zhao, Y. P. Wu, Z. J. Xiang, Z. C. Xia, A. F. Wang, X. G. Luo, T. Wu *et al.*, Phys. Rev. B **91**, 205133 (2015).
[8] Y. Nakajima, P. Syers, X. Wang, R. Wang, and J. Paglione, Nat. Phys. **12**, 213 (2016).
[9] S. Wolgast, Y. S. Eo, T. Öztürk, G. Li, Z. Xiang, C. Tinsman, T. Asaba, B. Lawson, F. Yu, J. W. Allen *et al.*, Phys. Rev. B **92**, 115110 (2015).

[10] D. J. Kim, S. Thomas, T. Grant, J. Botimer, Z. Fisk, and J. Xia, Sci. Rep. **3**, 3150 (2013).
[11] P. Syers, D. Kim, M. S. Fuhrer, and J. Paglione, Phys. Rev. Lett. **114**, 096601 (2015).
[12] N. Xu, P. K. Biswas, J. H. Dil, R. S. Dhaka, G. Landolt, S. Muff, C. E. Matt, X. Shi, N. C. Plumb, M. Radović *et al.*, Nat. Commun. **5**, 4566 (2014).
[13] N. Xu, X. Shi, P. K. Biswas, C. E. Matt, R. S. Dhaka, Y. Huang, N. C. Plumb, M. Radović, J. H. Dil, E. Pomjakushina *et al.*, Phys. Rev. B **88**, 121102 (2013).
[14] D. J. Kim, J. Xia, and Z. Fisk, Nat. Mater. **13**, 466 (2014).
[15] G. Li, Z. Xiang, F. Yu, T. Asaba, B. Lawson, P. Cai, C. Tinsman, A. Berkley, S. Wolgast, Y. S. Eo *et al.*, Science **346**, 1208 (2014).
[16] B. S. Tan, Y.-T. Hsu, B. Zeng, M. C. Hatnean, N. Harrison, Z. Zhu, M. Hartstein, M. Kiourlappou, A. Srivastava, M. D. Johannes *et al.*, Science **349**, 287 (2015).
[17] S. Biswas, R. Nagarajan, S. Sarkar, K. R. Amin, M. Ciomaga Hatnean, S. Tewari, G. Balakrishnan, and A. Bid, Phys. Rev. B **92**, 085103 (2015).
[18] S. Thomas, D. Kim, S. Chung, T. Grant, Z. Fisk, and J. Xia, Phys. Rev. B **94**, 205114 (2016).
[19] M. Neupane, N. Alidoust, S. Y. Xu, T. Kondo, Y. Ishida, D. J. Kim, C. Liu, I. Belopolski, Y. J. Jo, T. R. Chang *et al.*, Nat. Commun. **4**, 2991 (2013).
[20] E. Frantzeskakis, N. de Jong, B. Zwartsenberg, Y. K. Huang, Y. Pan, X. Zhang, J. X. Zhang, F. X. Zhang, L. H. Bao, O. Tegus *et al.*, Phys. Rev. X **3**, 041024 (2013).
[21] P. Hlawenka, K. Siemensmeyer, E. Weschke, A. Varykhalov, J. Snchez-Barriga, N. Shitsevalova, A. Dukhnenko, V. Filipov, S. Gabni, and K. Flachbart, arXiv:1502.01542.
[22] D.-X. Qu, Y. S. Hor, J. Xiong, R. J. Cava, and N. P. Ong, Science **329**, 821 (2010).
[23] C. Brüne, C. X. Liu, E. G. Novik, E. M. Hankiewicz, H. Buhmann, Y. L. Chen, X. L. Qi, Z. X. Shen, S. C. Zhang, and L. W. Molenkamp, Phys. Rev. Lett. **106**, 126803 (2011).
[24] I. Utke, S. Moshkalev, and P. Russell, *Nanofabrication Using Focused Ion and Electron Beams: Principles and Applications* (Oxford University Press, Oxford, 2012).
[25] P. Gabriel, G. Slavomír, F. Karol, F. Vladimir, and S. Natalya, JPS Conf. Proc. **3**, 012021 (2014).
[26] Z. Schlesinger, Z. Fisk, H.-T. Zhang, M. B. Maple, J. F. DiTusa, and G. Aeppli, Phys. Rev. Lett. **71**, 1748 (1993).
[27] T. Caldwell, A. P. Reyes, W. G. Moulton, P. L. Kuhns, M. J. R. Hoch, P. Schlottmann, and Z. Fisk, Phys. Rev. B **75**, 075106 (2007).
[28] L. Jiao, S. Rößler, D. J. Kim, L. H. Tjeng, Z. Fisk, F. Steglich, and S. Wirth, Nat. Commun. **7**, 13762 (2016).
[29] J. C. Cooley, M. C. Aronson, A. Lacerda, Z. Fisk, P. C. Canfield, and R. P. Guertin, Phys. Rev. B **52**, 7322 (1995).
[30] J. C. Cooley, C. H. Mielke, W. L. Hults, J. D. Goettee, M. M. Honold, R. M. Modler, A. Lacerda, D. G. Rickel, and J. L. Smith, J. Supercond. **12**, 171 (1999).
[31] K. Sugiyama, F. Iga, M. Kasaya, T. Kasuya, and M. Date, J. Phys. Soc. Jpn. **57**, 3946 (1988).
[32] M. Jaime, R. Movshovich, G. R. Stewart, W. P. Beyermann, M. G. Berisso, M. F. Hundley, P. C. Canfield, and J. L. Sarrao, Nature (London) **405**, 160 (2000).
[33] K. Flachbart, M. Bartkowiak, S. Demishev, S. Gabani, V. Glushkov, T. Herrmannsdorfer, V. Moshchalkov, N. Shitsevalova, and N. Sluchanko, Physica B (Amsterdam) **404**, 2985 (2009).
[34] J. Yong, Y. Jiang, X. Zhang, J. Shin, I. Takeuchi, and R. L. Greene, AIP Adv. **5**, 077144 (2015).
[35] J. W. Allen, B. Batlogg, and P. Wachter, Phys. Rev. B **20**, 4807 (1979).
[36] J. C. Cooley, M. C. Aronson, Z. Fisk, and P. C. Canfield, Phys. Rev. Lett. **74**, 1629 (1995).
[37] S. Wolgast, C. Kurdak, K. Sun, J. W. Allen, D.-J. Kim, and Z. Fisk, Phys. Rev. B **88**, 180405 (2013).
[38] F. Lu, J. Z. Zhao, H. Weng, Z. Fang, and X. Dai, Phys. Rev. Lett. **110**, 096401 (2013).
[39] X. Zhang, N. P. Butch, P. Syers, S. Ziemak, R. L. Greene, and J. Paglione, Phys. Rev. X **3**, 011011 (2013).
[40] G. Mihajlović, J. E. Pearson, M. A. Garcia, S. D. Bader, and A. Hoffmann, Phys. Rev. Lett. **103**, 166601 (2009).